

2016

The High Speed Planing Characteristics of A Rectangular Flat Plate of Fixed Trim and Draft

Man Gao

Lehigh University

Follow this and additional works at: <http://preserve.lehigh.edu/etd>



Part of the [Mechanical Engineering Commons](#)

Recommended Citation

Gao, Man, "The High Speed Planing Characteristics of A Rectangular Flat Plate of Fixed Trim and Draft" (2016). *Theses and Dissertations*. 2598.

<http://preserve.lehigh.edu/etd/2598>

This Thesis is brought to you for free and open access by Lehigh Preserve. It has been accepted for inclusion in Theses and Dissertations by an authorized administrator of Lehigh Preserve. For more information, please contact preserve@lehigh.edu.

**The High-Speed Planing Characteristics of A Rectangular Flat
Plate of Fixed Trim and Draft**

by

Man Gao

A Thesis

Presented to the Graduate and Research Committee

of Lehigh University

in Candidacy for the Degree of

Master of Science

in

Mechanical Engineering and Mechanics

Lehigh University

May, 2016

© (2016) Copyright
Man Gao

Thesis is accepted and approved in partial fulfillment of the requirements for the Master of Science in Mechanical Engineering Department.

THESIS TITLE: The High-Speed Planing Characteristics of A Rectangular Flat Plate of Fixed Trim and Draft)
YOUR NAME: Man Gao

Date Approved

Thesis Director

(Name of Co-Director)

(Name of Department Chair)

ACKNOWLEDGMENTS

I would like to express special appreciation to my advisor Professor Joachim Grenestedt, who has provided me with patient and professional guidance in my studies. With his kind instruction, I gained understanding about high-speed boats, hydrodynamic knowledge and ANSYS simulation. Professor Grenestedt always encouraged me to go deeper into my project and create something new despite the difficult road and obstacles along the way. I also appreciate Professor Alparslan Oztekin and his Ph.D student Yihan Liu who instructed me with the usage of FLUENT and VOF modelling.

Further, I would like to thank the numerous other faculty and staff from Lehigh University that helped me with this project. Without your contributions, I could not have finished this thesis.

Finally and most of all, I would like to thank my parents for their supports. They have provided me with confidence and continuous motivation. Thank you for your love.

CONTENTS

ACKNOWLEDGMENTS	iv
CONTENTS	v
LIST OF FIGURES.....	vii
LIST OF TABLES.....	vii
ACRONYMS.....	viii
NOMENCLATURE.....	ix
ABSTRACT.....	1
Chapter 1	2
1.1 Background	3
1.2 Purpose and Objectives	4
1.3 Method	4
Chapter 2	6
2.1 Basic Fluid Flow.....	6
2.1.1 The Mass Conservation Equation.....	7
2.1.2 Momentum Conservation Equation.....	7
2.2 Turbulence.....	8
2.2.1 Turbulence Flow	8
2.2.2 Turbulence Modeling	9
2.2.3 Boundary Layers.....	12
2.3 Free Water Surface.....	14
2.3.1 The Volume of Fluid Method.....	15
2.4 Non-Dimensional Coefficients.....	15
Chapter 3	16
Numerical Methods	16
3.1 The Finite Volume Method	16
3.2 VOF Discretization Schemes.....	17
3.3 Convergence Criteria	19
Chapter 4	20
CFD Simulation.....	20
4.1 Computational Domain Definition	20

4.2 Mesh Generation	22
4.3 Model Definition and Properties.....	24
4.4 Boundary Conditions	26
4.5 Solution	27
4.6 Post-Processing	28
4.7 Operating Conditions	28
Chapter 5	31
Results and Discussion	31
5.1 Planing Plate with 2° Trim Angle	32
5.2 Planing Plate with 4° Trim Angle	35
Chapter 6	37
Conclusion	37
Chapter 7	39
Future Work.....	39
Reference	40
Appendix A	42
The Mass Conservation Equation.....	42
Momentum Conservation Equation.....	42
Turbulence Modeling	43
Appendix B	49
Curriculum Vitae	51

LIST OF FIGURES

FIGURE 1.1: WORK FLOW OF THE CFD SIMULATION	5
FIGURE 2.1: SCHEMATIC ILLUSTRATION OF A BOUNDARY LAYER AT A FLAT SUBMERGED PLATE [4]	13
FIGURE 4.1: DIMENSIONS OF THE COMPUTATIONAL DOMAIN. THE PLANING PLATE IS AT THE ORIGIN; IT IS SUBSTANTIALLY SMALLER THAN THE COMPUTATIONAL DOMAIN AND THUS NOT VISIBLE IN THIS FIGURE.	21
FIGURE 4.2: ILLUSTRATION OF MESH	22
FIGURE 4.3: SIZING PLATE MESH	23
FIGURE 4.4: NAMED SELECTIONS IN MESH GENERATION	24
FIGURE 4.5: PHASE CONTOUR OF COMPUTATIONAL DOMAIN	27
FIGURE 4.6: THE DIMENSIONS OF THE PLATE WITH 2° TRIM	29
FIGURE 4.7: VOLUME FRACTION CONTOUR OF LM/B=3 AT T=0.0956S	29
FIGURE 5.1: FLOW PATTERN AT LOW TRIMS [3]	31
FIGURE 5.2: FLOW PATTERN OF PLATE WITH 4° TRIM (LM/B=4.5, CV=12.5, T=1.5S)	32
FIGURE 5.3: CONTOUR OF VELOCITY AT T=0.088S, CV=12.5, LM/B=1.5	33
FIGURE 5.4: DRAG VS LIFT FOR THE PLATE WITH 2° TRIM ANGLE. COMPARISON OF NACA AND FLUENT DATA.	34
FIGURE 5.5: WAVE ELEVATION CONTOUR AT T=1.5S, CV=12.5, LM/B=1.5	35
FIGURE 5.6: 4° TRIM ANGLE DRAG VS LIFT COEFFICIENT, COMPARISON BETWEEN NACA AND FLUENT.	36
FIGURE 6.1: NACA SETUP OF MODEL AND TOWING GEAR [3]	38

LIST OF TABLES

TABLE 4.1: SOLVER SETTINGS	25
TABLE 4.2: FLUID PROPERTIES	26
TABLE 4.3: PHASES	26
TABLE 4.4: SIMULATED CASES OPERATION CONDITIONS	30
TABLE 5.1: 2° ANSYS SIMULATION RESULT	34
TABLE 5.2: 4° ANSYS SIMULATION RESULT	36

ACRONYMS

CAD	Computer-Aided Design
CFD	Computational Fluid Dynamics
DNS	Direct Numerical Simulation
EFD	Experimental Fluid Dynamics
FVM	Finite Volume Method
GCI	Grid Convergence Index
HRIC	High Resolution Interface Capturing Scheme
PDE	Partial Difference Equation
RANS	Reynolds Average Navier-Stokes Equation
SIMPLE	Semi-Implicit Method for Pressure Linked Equations
SST	Shear Stress Transport
VOF	Volume of Fluid

NOMENCLATURE

b	Beam of Planing Surface, m
d	Draft at Trailing Edge (measured vertically from undistributed water level), m
F	Friction, parallel to planing surface, N
g	Acceleration due to Gravity, 9.81m/s ²
l _m	Mean Wetted Length, m
D	Drag Force, N
Re	Reynolds Number, $V_m l_m / \nu$
C _v	Speed Coefficient or Froude Number, V / \sqrt{gb}
C _{Lb}	Lift Coefficient based on Square of Beam, $\frac{F}{\frac{\rho}{2} V^2 b^2}$
C _{Db}	Drag Coefficient based on Square of Beam, $\frac{D}{\frac{\rho}{2} V^2 b^2}$
τ	Trim Angle between Horizontal and Planning Bottom, deg
ν	Kinematic viscosity, m ² /s
S _m	Mass Added to the Continuous Phase from Dispersed second phase
$\bar{\tau}$	The Stress Deviator Tensor
\bar{U}_t	Time Averaged Velocity
\bar{P}	Time Averaged Pressure

u_i	Fluctuating Components of Velocity
P	Fluctuating Components of Pressure
K	Turbulent Kinetic Energy
ω	Turbulent Specific Dissipation
y^+	Dimensionless Wall Distance
y	Distance to the wall
u_*	Friction Velocity
τ_ω	Wall Shear Stress
ϕ	Convection of a General Flow Variable
ϕ_P	Flow Variable in the Present Cell
ϕ_{nb}	Values of the Flow Variable in the Neighboring Cells
a_P	Discretization Coefficient Associated to the Present Cell
a_{nb}	Discretization Coefficients Describing the Interaction with its Neighboring Cells

ABSTRACT

The High-Speed Planing Characteristics of A Rectangular Flat Plate Over A Wide Range of Trim and Draft

Man Gao

Lehigh University, 2016

Director: Professor Joachim L. Grenestedt

Numerical analyses of a flat planing plate in a towing tank were performed using the ANSYS Fluent software package. The flat plate represented a simple version of a sponson for a suspension boat. Analyses were performed for different trim angles, draft at the trailing edge, and speed. The results were compared to published experimental data. The agreement was in general fair (on the order of 10%).

Chapter 1

Introduction

There is presently extensive interest in so-called suspension boats, consisting of an airborne center hull connected via suspension links to multiple sponsons. The sponsons are planing on the water and provide lift to the boat. Lift and drag characteristics of the sponsons are of major importance. The goal of the present project was to estimate lift and drag forces of a simple planing surface using computational fluid dynamic (CFD) and to compare with published experimental data. The hope is to use CFD in the future to assist in the design of real sponsons for manned or unmanned suspension boats.

The National Advisory Committee for Aeronautics, NACA, undertook an experimental investigation of high-speed planing characteristics for a series of prismatic surfaces [3]. The purpose of that investigation was to extend the available data to high speed, high trim and long wetted lengths. However, experimental methods are time consuming and expensive, in particular when it is desirable to study a wide range of geometries. It would be very beneficial if computational fluid dynamics (CFD) could be used to predict the planing characteristics of various sponson designs, rather than having to rely on making physical models and testing them in a tow tank.

1.1 Background

Planing characteristics research has traditionally relied on model scale experiment in towing tanks. However, in the last few decades many numerical studies on planing hulls have been performed. Brizzolara and Serra [10] compared CFD simulation results of planing, hulls using the Savitsky method, with experimental data. There are many advantages to using Computational Fluid Dynamics (CFD) in the first phase when designing a hull, and consequently CFD has been widely accepted as a simulation and optimization tool in many industrial branches. When it comes to designing hulls, the most important aspects of using CFD techniques are the ability to handle complex geometry with relevant details, the efficient simulation process (from geometry to solution, parametric studies, optimization studies, user interface), the adequate models of turbulence and free-surface effects, the coupled simulation of flow and flow-induced motion.

Recent studies show that CFD simulations of displacement hulls have been made with a precision that begins to approach the results of towing tank tests. In 2010, at the workshop on numerical Ship Hydrodynamics in Gothenburg, 33 groups performed simulations of three large displacement ships [14]. The results from all groups showed that the average error of the predictions in comparison to towing tank experiments was only 0.1% with a standard deviation of 2.1%. However the prediction of sinkage and trim were less accurate for the higher speed; the mean error was around 4%.

1.2 Purpose and Objectives

The purpose of this study was to evaluate the accuracy of CFD using the commercially available software ANSYS (FLUENT), with the long term objective of fully or partially replacing towing tank tests in planning hull design. This was implemented by calculating the drag and lift for given speed, draft and trim angle of a planing plate, and comparing the numerical results with the experimental data from NACA [3].

1.3 Method

The flow diagram shown below outlines the general work flow of the present CFD simulation. The simulation process begins by defining the computational fluid domain where analysis are performed, and then generates the computational meshes to separate the domain into cells. Models for the flow are chosen in the next step, and then boundary conditions are defined. Finally, the mathematical problem is solved. After the calculations have finished, the results were analyzed in the post processing step. These steps are made in an iterative process where the results are evaluated and further simulations are performed.

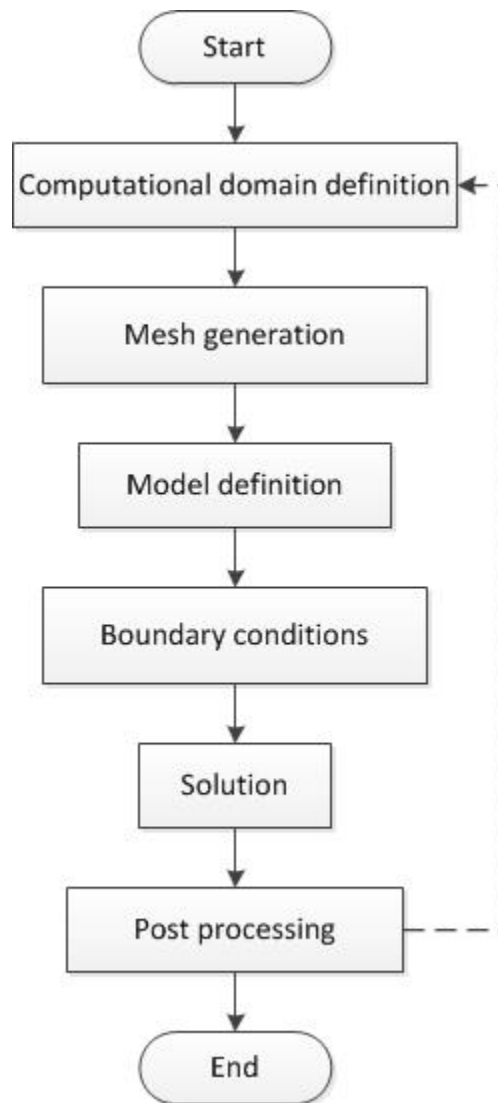


Figure 1.1: Work Flow of the CFD Simulation

Chapter 2

Theory

This chapter mainly provides the theoretical background that supports the remainder of the report. It starts with the introduction of the basic flow used in the report and continues with describing the mathematic models used in the simulation of the plate in motion.

2.1 Basic Fluid Flow

ANSYS FLUENT provides comprehensive modeling capabilities for a wide range of flow regimes, including incompressible and compressible flow as well as laminar and turbulent fluid flow problems. Steady or transient state analysis can also be performed. To perform the simulation in this case, we chose to use incompressible, turbulent and transient state flow model with gas-liquid transportation model. ANSYS FLUENT solves conservation equations for mass and momentum for all flows. This case was also solved based on the two basic conservation equations. The detailed equations are presented in Appendix A. In this section, the conservation equations for the flow in an inertial reference frame are stated.

2.1.1 The Mass Conservation Equation

The appropriately simplified equation for conservation of mass, for the 3-D Cartesian coordinate system employed in this analysis in this case can be written as:

$$\frac{\partial}{\partial x}(\rho v_x) + \frac{\partial}{\partial y}(\rho v_y) + \frac{\partial}{\partial z}(\rho v_z) = S_m \quad (2.1)$$

Where x , y , z are the Cartesian coordinates, and v_x , v_y , v_z are components of velocity.

Equation 2.1 is the form of the mass conservation equation applied in this study. The term S_m is the mass added to the continuous phase from the dispersed second phase (water) mass flow patched on to the primary phase (air).

2.1.2 Momentum Conservation Equation

Conservation of momentum in an inertial (non-accelerating) reference frame is described as [4]:

$$\frac{\partial}{\partial t}(\rho \vec{v}) + \nabla \cdot (\rho \vec{v} \vec{v}) = -\nabla p + \nabla \cdot (\vec{\tau}) + \rho \vec{g} + \vec{F} \quad (2.2)$$

Where p is the static pressure, $\vec{\tau}$ is the stress deviator tensor (described in Appendix A), $\rho \vec{g}$ is the gravitational body force and \vec{F} is the force that arises from interaction with the dispersed phase [13].

2.2 Turbulence

When the plate is moving through water at high speed, the flow around the plate is in a turbulent state. In this section, the governing equations applied to this model for turbulent flows are presented, and turbulence modeling is explained.

2.2.1 Turbulence Flow

Turbulence is characterized as a three-dimensional irregular flow where turbulent kinetic energy (set as $0.001 \text{ m}^2/\text{s}^2$ in the initialization) is dissipated from the largest to the smallest turbulent scales. On the smallest turbulent scales, which are called Kolmogorov scales, the energy is dissipated into heat due to viscous forces. Since turbulence is a dissipative phenomenon, energy must be continuously supplied in order to maintain a turbulent flow.

The motion of a viscous fluid is governed by the Navier-Stokes equations, which can be used in both laminar and turbulent flow. As supposed in this case both phases are incompressible (the Mach number of air in this case is 0.036 which is lower than 0.3 so we make the assumption that the air is incompressible), Newtonian fluid in three dimensional space under the effect of gravitational field, the N-S equations are transformed according to the model as:

$$\frac{\partial U_i}{\partial t} + U_j \frac{\partial U_i}{\partial x_j} = -\frac{1}{\rho} \frac{\partial P}{\partial x_i} + \nu \frac{\partial^2 U_i}{\partial x_j \partial x_j} + g_i \quad (2.3)$$

The equations are formulated using tensor notation. The indices i and j in the N-S equations run over the spatial coordinated x , y and z . In these equations, U_i is the velocity component in direction i , x_i is the spatial coordinate in dimension i , t is time, ρ is the density, P is the pressure, ν is the kinematic viscosity and g_i is the gravitational acceleration.

Analytical solutions of Navier-Stokes equations only exist for some very limited cases. For turbulent flows in real engineering applications, analytical solutions in general do not exist. The Navier-Stokes equation must then be solved by numerical methods.

2.2.2 Turbulence Modeling

The traditional method to resolve turbulent flow regime problems is to use turbulence models in which the features of turbulent flow are not solved in time. Through conducting Reynolds decomposition, the instantaneous velocity and pressure can be decomposed into two parts [5]: the time averaged quantities and the fluctuating parts (see Appendix A). By inserting the Reynolds decomposition into the N-S equations, the Reynolds averaged N-S (RANS) equations are obtained as follows:

$$\bar{U}_j \frac{\partial \bar{U}_i}{\partial x_j} = -\frac{1}{\rho} \frac{\partial \bar{P}}{\partial x_i} + \nu \frac{\partial^2 \bar{U}_i}{\partial x_j \partial x_j} - \frac{\partial \overline{u_i u_j}}{\partial x_j} + g_i \quad (2.4)$$

Where \bar{U}_i and \bar{P} are the time averaged quantities while u_i and p are the fluctuating components of the velocities and the pressure. The RANS transform equations are

similar to N-S equations except for the additional term, $\overline{u_i u_j}$, referred to as the Reynolds stress tensor. By modelling the Reynolds Stress tensor, the RANS equations describe the time averaged flow quantities which require substantially less computational resources than the DNS scenario.

The approach used for modelling the Reynolds stress tensor of the RANS equations is to use the Boussinesq approximation (see Appendix A).

By using a model to describe how the turbulent viscosity depends on the flow, the RANS equations can be solved. The two-equation turbulence models, such as the k- ϵ model and the k- ω model, use two additional transport equations to describe the turbulent viscosity. They are referred to as complete models since they allow the turbulent velocity and length scales to be described independently [15].

2.2.2.1 The Standard k- ϵ Model

The standard model in ANSYS FLUENT falls within this class of models and has become the workhorse of practical engineering flow calculations since it was proposed by Launder and Spalding. [5] The standard k- ϵ model is based on model transport equations for the turbulence kinetic energy (k) and its dissipation rate (ϵ). The equations are demonstrated in Appendix A.

The standard $k-\varepsilon$ model is robust and works well in predicting free flows with small pressure gradients. It is based on the assumption that the flow is fully turbulent which means the applications are limited to high Reynolds number flows [11]. Over time, it has been proven that the standard $k-\varepsilon$ model cannot be used to describe the wave behind moving hull in a satisfactory manner [11].

2.2.2.2 The $k-\omega$ Model

In the $k-\omega$ model described by Wilcox [6], the transport equations for the turbulent kinetic energy and its specific dissipation, ω , are used in a similar way as for the standard $k-\varepsilon$ model. The specific dissipation is related to the dissipation according to

$$\omega \propto \frac{\varepsilon}{k} \quad (2.5)$$

The model equations for k and ω are demonstrated in Appendix A.

The $k-\omega$ model has the advantage that it is also valid close to walls and in regions of low turbulence which means that the transport equations can be used in the whole flow domain. A disadvantage of the $k-\omega$ model is that the results are easily affected by the choice of boundary conditions and initial states.

2.2.2.3 The SST k- ω Model

Menter [6] developed the shear stress transport (SST) model by combining the advantages of the k- ϵ and the k- ω models into one using blending functions. In this hybrid model, the k- ω model is used along the boundary layer while the k- ϵ model, formulated on k- ω form, is used in the open channel free flow.

The SST k- ω model has been proven good performance in many types of complex flows, such as flows with adverse pressure gradients and separating flows. The flows using the k- ϵ or the k- ω models have given results that differ significantly from experimental data. It has been recognized for its good overall performance and it is the most commonly used turbulence model for simulations of hydrodynamics and was adopted in this case as well.

2.2.3 Boundary Layers

When a fluid flows along a surface, shear stresses give rise to a boundary layer in the vicinity of the surface. The schematic of a boundary layer near the edge of a fully submerged flat plate is illustrated in Fig 2.1 [8], where the incident flow has a uniform velocity profile with velocity U_0 . When the flow reaches the plate, a laminar boundary layer starts to grow at the surface. After some distance, the boundary layer goes into a

transitional region after which a turbulent boundary layer is developed. The flow in the inner part of the turbulent boundary layer is developed.

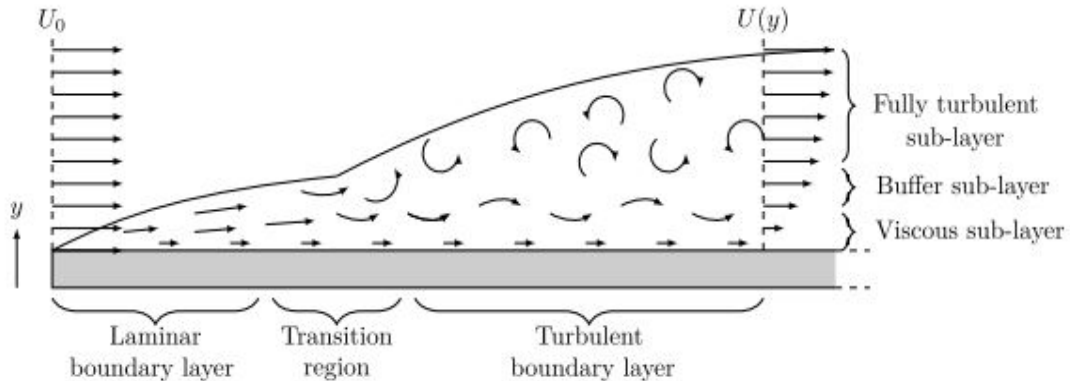


Figure 2.1: Schematic illustration of a boundary layer at a flat submerged plate [4]

In the boundary layer, the gradients of the flow variables in the normal direction are generally very large in comparison to those of the free flow. This implies that a high spatial resolution is required by the solution method in order to capture the effects near the wall. A common alternative method used to circumvent the requirement of a high spatial resolution is to use wall functions, which are empirical models used to estimate the flow variables near walls.

Standard wall functions are based on the assumption that the boundary layer can be described as a flat plate boundary layer. This means that the time-averaged velocity can be expressed as a function of the dimensionless wall distance. In the viscous sub-layer, it can be shown that the velocity parallel to the wall is proportional to y^+ . In the fully

developed turbulent sub-layer, the velocity follows the logarithm of y^+ . Between these sub-layers, in the buffer sub-layers, there is a transitional region from linear to logarithmic y^+ dependence. In order for a wall function to work properly, it should be used through the fully turbulent layer which corresponds to a value of y^+ above 30.

It is important that the mesh near the wall is properly sized to ensure accurate simulation of the flow field, a dimensionless wall distance y^+ is introduced to help determine the mesh size; a detailed description is provided in Appendix A. The desired y^+ can be calculated by equations in Appendix A based on flow properties and initial velocity. Then proper wall distance y can be estimated which is an indicator if the mesh is able to resolve the boundary layer appropriately [11]. The exact y^+ value can only be calculated after the CFD simulation, since the actual boundary layer profile is needed for this.

2.3 Free Water Surface

In order to simulate the planing plate in water, models should resolve the interface between the water and air. There are some different two-phase models available that either tracks the surface directly or tracks the different phases and then reconstructs the interface. The most frequently used method to capture the free surface in ship hydrodynamics appears to be the volume of fluid (VOF) method. In the VOF method, the different phases are tracked.

2.3.1 The Volume of Fluid Method

In the VOF method, each phase is marked with a color function, γ , which is the volume fraction of one of the phases. If only one phase is present, meaning that γ is either 0 or 1, the ordinary Navier-Stokes equations are solved. If $0 < \gamma < 1$, there is an interface present and the properties of the phases are averaged in order to get a single set of equations. The average density and viscosity are:

$$\rho = \gamma\rho_1 + (1 - \gamma)\rho_2 \quad (2.6)$$

$$\nu = \gamma\nu_1 + (1 - \gamma)\nu_2$$

2.4 Non-Dimensional Coefficients

For comparison of the speed, drag and lift, these quantities can be scaled by dimensionless numbers. The speed coefficient is defined as:

$$C_V = V/\sqrt{gb} \quad (2.7)$$

The lift coefficient based on the square of the beam is defined as:

$$C_{Lb} = \frac{L}{\frac{\rho}{2}V^2b^2} \quad (2.8)$$

The drag coefficient based on square of the beam is defined as:

$$C_{Db} = \frac{R}{\frac{\rho}{2}V^2b^2} \quad (2.9)$$

Where b (m) is the beam of the planing surface; R (N) is drag, L (N) is lift, ρ (kg/m^3) is density of water, g (m/s^2) is gravitational acceleration, and V (m/s) is velocity of the planing plate.

Chapter 3

Numerical Methods

In this chapter, the numerical methods used for solving the mathematical models introduced in Chapter 2 are described.

3.1 The Finite Volume Method

The finite volume method (FVM) is a numerical method of discretizing a continuous partial differential equation (PDE) into a set of algebraic equations. The first step of the discretization is to divide the computational domain into a finite number of volumes, forming what is called a mesh. Next the PDE is integrated in each volume by using the divergence theorem, yielding an algebraic equation for each cell. In the centers of the cells, cell-averaged values of the flow variables are stored in so called nodes. This implies that the spatial resolution of the solution is limited by the cell size since the flow variables do not vary inside a cell. The FVM is conservative, meaning that the flux leaving a cell through one of its boundaries is equal to the flux entering the adjacent cell

through the same boundary. This property makes it advantageous for problems in fluid dynamics (see Appendix B).

The discretization coefficients depend on the discretization schemes used to approximate the values of the flow variables on the cell boundaries, also known as cell faces. By using appropriate discretization schemes to determine the coefficients of equations, a set of algebraic equations for the cell values is obtained.

3.2 VOF Discretization Schemes

The convection and diffusion terms are discretized using different numerical schemes that estimate the face values of the flow variables. Most often, diffusion terms are discretized by using a central differencing scheme where the face values are calculated by interpolation between the closest cells. In order to discretize the convection terms, the flow direction has to be taken into account. The simplest way is to let the face value between two cells be equal to the value of the first upstream cell which is done in the first order upwind scheme. In the second order upwind scheme, the face value is calculated from the two closest upwind cells.

It is often recommended to start a numerical simulation process with lower order schemes, such as the first order upwind scheme, to ensure stability [15]. However, the low accuracy of these schemes can lead to a high degree of unphysical diffusion in the

solution, known as numerical diffusion [15]. When the flow field has started to settle, higher order schemes should therefore be used to obtain more physically correct results. The second order upwind scheme is often considered as a suitable discretization scheme since it exhibits a good balance between numerical accuracy and stability [15].

The main problem related to the VOF model is to discretize the convection term in the transport equation for the color function in order to achieve a sharp interface [16]. The color function, γ , has to be between 0 and 1. Lower order numerical schemes are bounded but will smear out the interface due to numerical diffusion while higher order schemes are more accurate but less stable. A combination of higher and lower order of schemes is often used such as HRIC in FLUENT.

3.2.1 Modified HRIC Scheme

The high resolution interface capturing scheme (HRIC), described by Muzaferija [15], uses a combination of upwind and downwind interpolation. The binding of the scheme in each cell is a function of the volume fraction distribution over the neighboring cells. The value of the flow variables is then corrected by the local value of the Courant number [15], which is a measure of how much of one fluid that is available in the donor cell. This is done in order to prevent more fluid flowing out of a cell in one time step than what was available in the previous time step. In order to prevent this interface becomes aligned with the numerical grid. Another correction is introduced to account

for the relative position of the free surface to the cell face. This is done by calculating the angle between the normal to the interface and the cell face normal.

This is used as the intermediate transient flow behavior is not the emphasis of this simulation, and the final steady-state solution is not affected by the initial flow conditions and there is a distinct inflow boundary for each phase [16].

3.2.2 Compressive Scheme

The compressive scheme is a discretization scheme where the numerical order of accuracy can be varied by using a so called slope limiter in the range between 0 and 2. For low values of the slope limiter, first and second order schemes are used. For values above 1, higher order schemes are incorporated [15].

3.3 Convergence Criteria

To be able to decide if a solution has reached a desirable level of convergence it is useful to monitor the residuals of the flow variables in each iteration. A residual is a measure of the imbalance between the left and right hand sides of a discretized transport equation. Convergence monitor using residual history was used [16]. An unscaled residual, R_ϕ , of a solution can thereby be obtained by calculating the sum of the residuals in all cells (Appendix B).

Chapter 4

CFD Simulation

In this chapter, the methodology used in the CFD analysis is described. The procedure follows the steps in Fig 1.1, including the computational domain definition, mesh generation, model definition, boundary conditions, solution and post processing. At the end, a section presenting the simulated operating conditions is included.

4.1 Computational Domain Definition

A large domain was created in order to reduce the influence of the no-slip boundaries on the flow. The domain was defined as an open channel with water underneath and air above. The NACA experiment was conducted at Langley Aeronautical Laboratory [3]. The NACA towing tank has the following dimensions [6]: 890 m in length, 7.315m in width and 3.962 m in depth. Motivated by the blockage theory [1], the simulation domain of 30 meters in length, 3.962 meters in water depth, and 7.315 meters in width was chosen. An air layer of 1.524 meters thickness was added above the water. In Figure 4.1, the computational domain was illustrated. The horizontal distance between the inlet wall of the tank and the yz plane was 10m, while the horizontal distance between the outlet wall of the tank and the yz plane was 20m, which shows in the Fig 4.1. The height of the domain was 5.486m. The draft at the trailing edge of the plate was defined as the

vertically depth from undistributed water level to the trailing edge. The wetted length in the NACA experiment was defined as the length from the trailing edge of the model to the intersection of the heavy spray line with the planing bottom.



Figure 4.1: Dimensions of the computational domain. The planing plate is at the origin; it is substantially smaller than the computational domain and thus not visible in this figure.

The model of the plate with different trim angles was created in the SolidWorks CAD program. After the plate geometry had been imported to the ANSYS geometry software, it was rotated and translated in order to obtain the desired draft at the trailing edge and trim angle. The fluid domain was created by subtracting the plate's geometry from the initial fluid domain. The origin was positioned at the undisturbed free surface level and horizontally aligned with the center of gravity of the plate.

4.2 Mesh Generation

The quality of the mesh plays a significant role in the accuracy and stability of the numerical computation. The main attributes associated with mesh quality are node point distribution, smoothness, and skewness [16]. To capture the important flow phenomena in the simulations, the mesh density was focused on certain regions of the domain.

The meshing process was divided into two parts. First, a Cut Cell assembly meshing was applied on the whole domain. The water and the air in the tank were divided into cubic cells. The minimum size of cube cell edges was adjusted to 10^{-3} m and the maximum size was adjusted to 0.128m. The Proximity and Curvature advanced size function was turned on with high smoothing chosen to assure smooth connection between cells. The default proximity accuracy was used. In Fig. 4.2 the mesh is shown. A total of 727687 nodes and 682476 elements were generated in the fluid region.

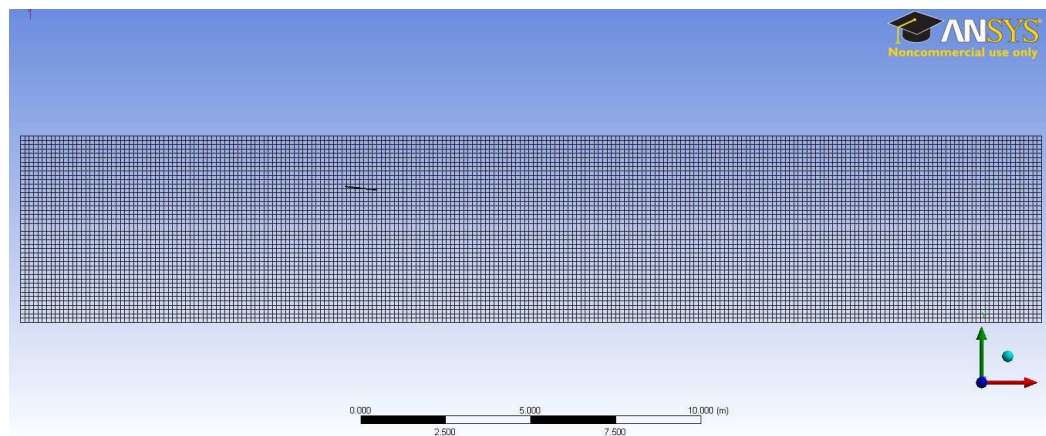


Figure 4.2: Illustration of mesh

Second, a sizing mesh control was added to six surfaces (shown in Fig. 4.4) of the plate to refine the meshing on the plate. The final simulation result would be greatly affected by the nodes and elements thickness near the plate. Fig. 4.3 illustrates the zoom in view of sizing control over the plate. The plate was named by selecting its six surfaces. The drag and lift forces were defined as the force components in the x and y directions of the plate.

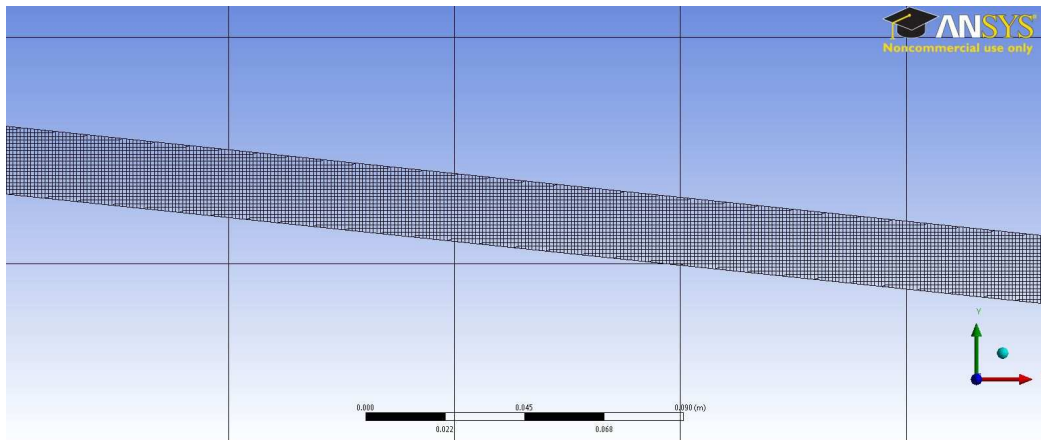


Figure 4.3: Sizing plate mesh

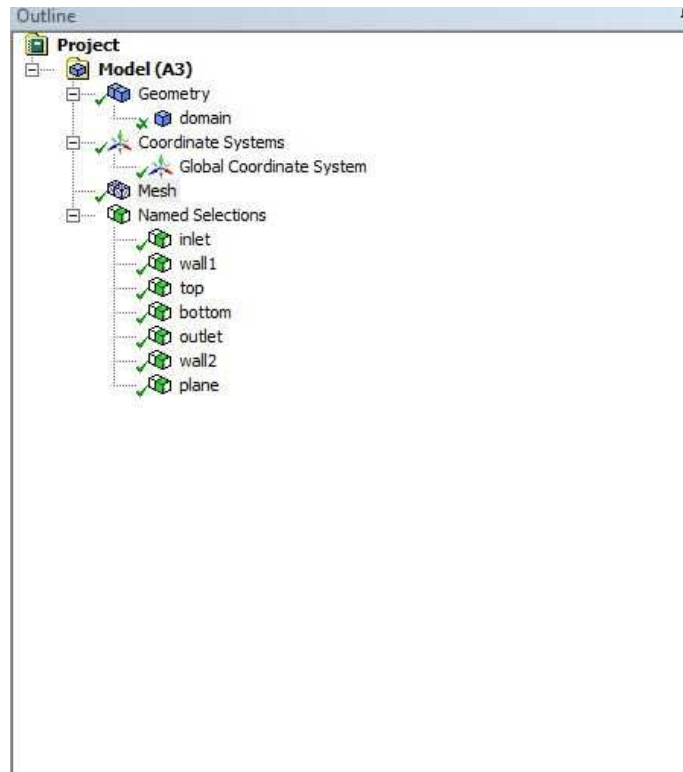


Figure 4.4: Named selections in mesh generation

4.3 Model Definition and Properties

This section describes the mathematical models and numerical methods used in the CFD simulations. Based on the theoretical background presented in Chapter 2, appropriate models were chosen for the simulations (Table 4.1). The VOF model was used for analyzing the two phase flow and the interaction between the flow and the plate. The turbulence was modelled using the time averaged RANS equations with the SST $k-\epsilon$ turbulence model. Standard wall functions were used in order to avoid resolving the whole boundary layer. The free surface was modelled and resolved with the VOF method. The fluid properties (Table 4.2) were set the same as in the model experiments,

[3], that were used to validate the results. Both the air and water were assumed to be incompressible, a simplification which appears reasonable due to the relatively low speeds (low Mach numbers). The primary phase was set as air while the secondary phase was set as water (Table 4.3).

After the physical models had been chosen, numerical methods were selected in the software. When choosing spatial discretization schemes, the second order upwind scheme was chosen for all convection terms except for the volume fraction equation, where the Modified HRIC scheme was used in FLUENT [9]. The diffusion terms were discretized with the central difference scheme. Since the steady behavior of the plate was simulated and temporal accuracy was not important, the first order implicit scheme was chosen in the temporal discretization [6] (Table 4.1).

Solver	Implicit, Segregated 3D
Scheme	SIMPLE
Gradient	Green-Gauss Cell Based
Pressure	PRESTO!
Momentum	Second Order Upwind
Volume Fraction	Modified HRIC
Turbulent Kinetic Energy	First Order Upwind
Specific Dissipation Rate	First Order Upwind
Intermittency	First Order Upwind
Momentum Thickness Re	First Order Upwind
Multiphase Model	Volume of Fluid
Near Wall Treatment	Standard Wall Functions

Table 4.1: Solver Settings

For Air	
Fluid Density	1.225 kg/m ³
Viscosity	1.7894e-05 kg/m·s
For Water	
Fluid Density	998.2 kg/m ³
Viscosity	1.3678e-03 kg/m·s

Table 4.2: Fluid Properties

Primary Phase	Air Phase
Secondary Phase	Water Phase

Table 4.3: Phases

4.4 Boundary Conditions

The phase contour of the computational domain is illustrated in Figure 4.5. The blue part on the bottom was water and the red part on the top was air. The top of the domain was defined as free slip walls. The bottom and both sides of the domain should have been free slip walls, but were incorrectly defined as no slip walls. It was a mistake; however, the influence on the results is believed to be negligible due to the width of the tank being much larger than the size of the planing plate. The inlet boundary condition was specified at the front of the domain set as a constant mass flow. The FLUENT option "Open Channel Boundary Condition" was selected. The free surface level and the bottom level of the water were defined. Mass flow rates (kg/s) of air and water were set in the inlet boundary settings. The velocity of the air was set the same as the water speed. The turbulent flow variables were set by specifying values of the turbulent intensity and turbulent viscosity ratio. The outlet, defined at the rear of the domain, was

set as a pressure outlet and the density interpolation method was set as neighboring cell volume fraction which levels were the same as the inlet boundary conditions.

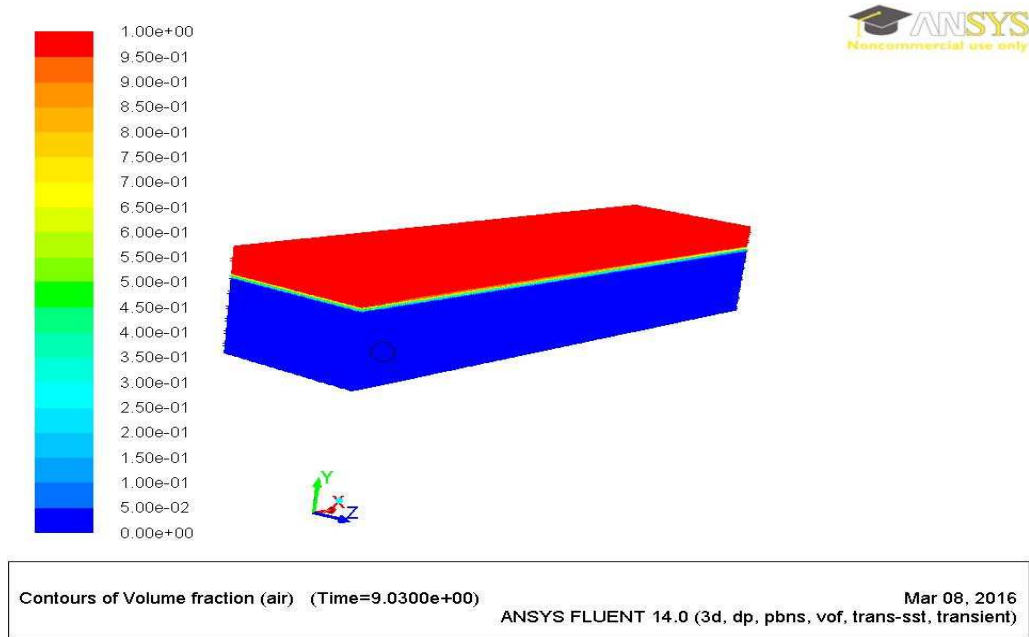


Figure 4.5: Phase contour of computational domain

4.5 Solution

The iterative procedure required that all solution variables are initialized before calculating a solution. Realistic guesses improves solution stability and accelerate convergence [16]. Initial x-direction velocity of air was applied on the air phase. Although a steady state solution was desired, transient simulations were run to increase the robustness of the solution [15]. The lift and drag oscillated for some time before settling down and converging to relatively steady values. The reported lift and drag are time averages towards the end of the simulations.

4.6 Post-Processing

After results had been obtained from the simulations, they were analyzed and compared and new simulations were devised. In this iterative procedure, appropriate settings for the simulations were found.

4.7 Operating Conditions

The CFD simulations were performed for two different trim angles, 2° and 4° , under different initial draft and speed. Fig. 4.6 shows the sketch of 2° plate, the gravitational center of which was the origin of the Cartesian coordinate system. The different draft at the trailing edge of each case was adjusted through altering the free surface level and the marked water area patched after initializing. The time step size was set at 0.0015 s, which appeared sufficiently short to allow good convergence. A total of 1000 time steps were run during each calculation, resulting in each simulation corresponding to 1.5 s. This appeared sufficient to reach steady state. Fig. 4.7 shows the draft projection on a plate at 0.0956 s. The detailed operation conditions are demonstrated in the Table 4.4 below.

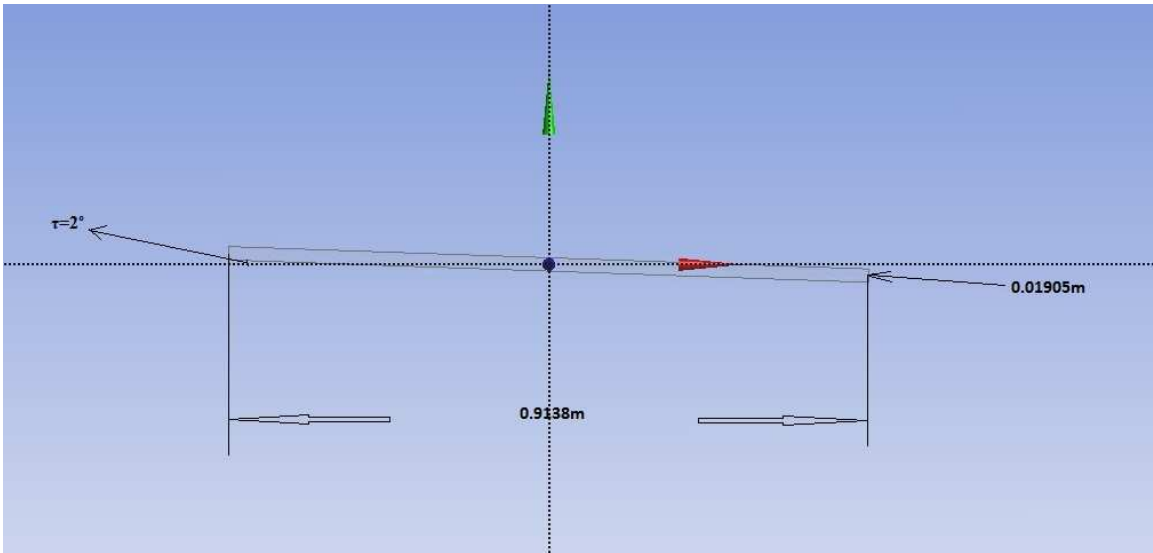


Figure 4.6: The dimensions of the plate with 2° trim.

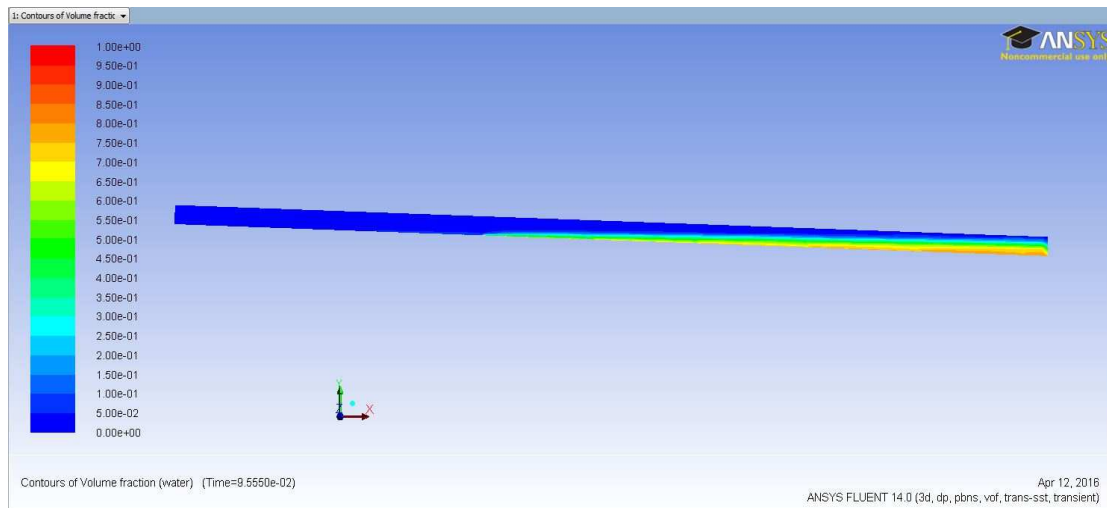


Figure 4.7: Volume fraction contour of $l_m/b=3$ at $t=0.0956s$

No.	Trim τ [deg]	Normalized Draft Im/b	Velocity Coefficient C_v
1	2°	1.5	12.5
2	2°	3	12.5
3	2°	4.5	12.5
4	2°	6	12.5
5	2°	7.5	12.5
6	2°	3	21.7
7	4°	1.5	12.5
8	4°	3	12.5
9	4°	4.5	12.5
10	4°	6	12.5
11	4°	7.5	12.5

Table 4.4: Simulated cases operation conditions

Chapter 5

Results and Discussion

This chapter presents the results from the CFD simulations as described in Chapter 4. As a convergence criterion, residuals were set to be less than $1e-6$. The iteration process converged well, as indicated by tracking the residuals through the iterations. The results were divided into two groups: a plate with 2° trim angle, and a plate with 4° trim angle; both with fixed draft at the trailing edge. The schematic flow pattern is shown in Fig. 5.2. When the trim angle is low like the cases simulated in this thesis, water would pile up under the planing bottom, as shown in Fig. 5.2 ($l/b=4.5$, $C_v=12.5$, $t=1.5s$). Drag and Lift coefficients (as defined in equations (2.8 and 2.9) and NACA [3]) on the plate were calculated from the forces from the simulations. Drag versus lift was plotted together with experimental data. The lowest drag for a given lift may be the optimal planing surface for a suspension boat.

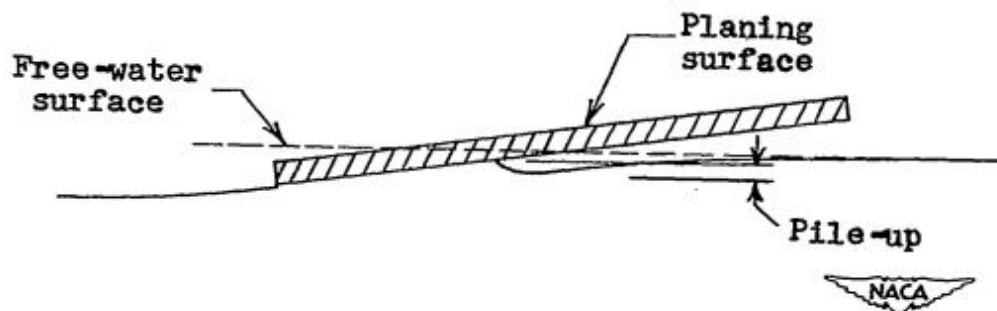


Figure 5.1: Flow pattern at low trims [3]

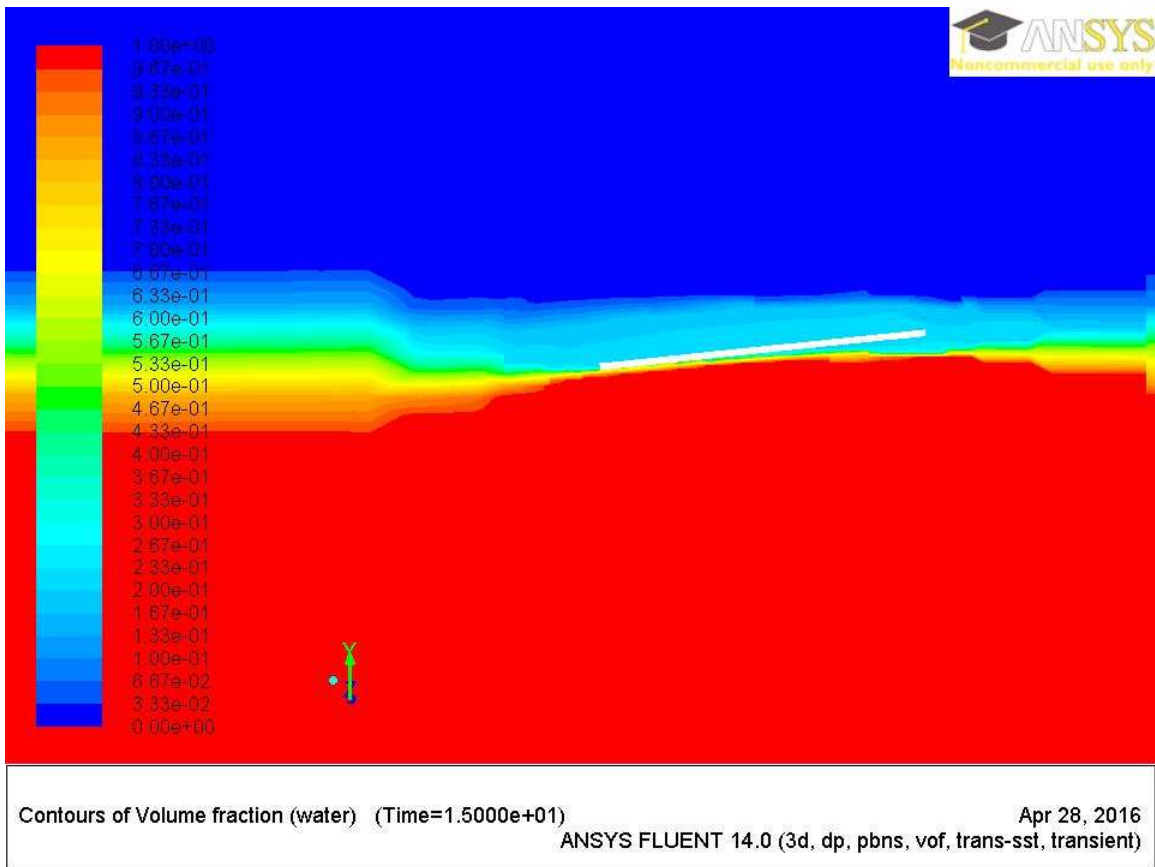


Figure 5.2: Flow pattern of plate with 4° trim ($l_m/b=4.5$, $C_v=12.5$, $t=1.5s$)

5.1 Planing Plate with 2° Trim Angle

In this section, the results from the simulations in ANSYS FLUENT of the 2° trim angle plate with fixed initial draft at the trailing edge are presented and compared with the NACA experimental data [3]. The cases were performed under different operating conditions. Fig.5.4 shows the velocity contour of case No. 5 at $t=0.088$. The comparison between the ANSYS simulation results and NACA experimental data is presented in

Figure 5.4 and Table 5.1. NACA experiments were performed under two different water viscosities which were marked separately in Table 5.1. Fluent simulations were performed with the viscosity 0.0013678 kg/m·s. Figure 5.4 indicates that the experimental and computational values are closely matching.

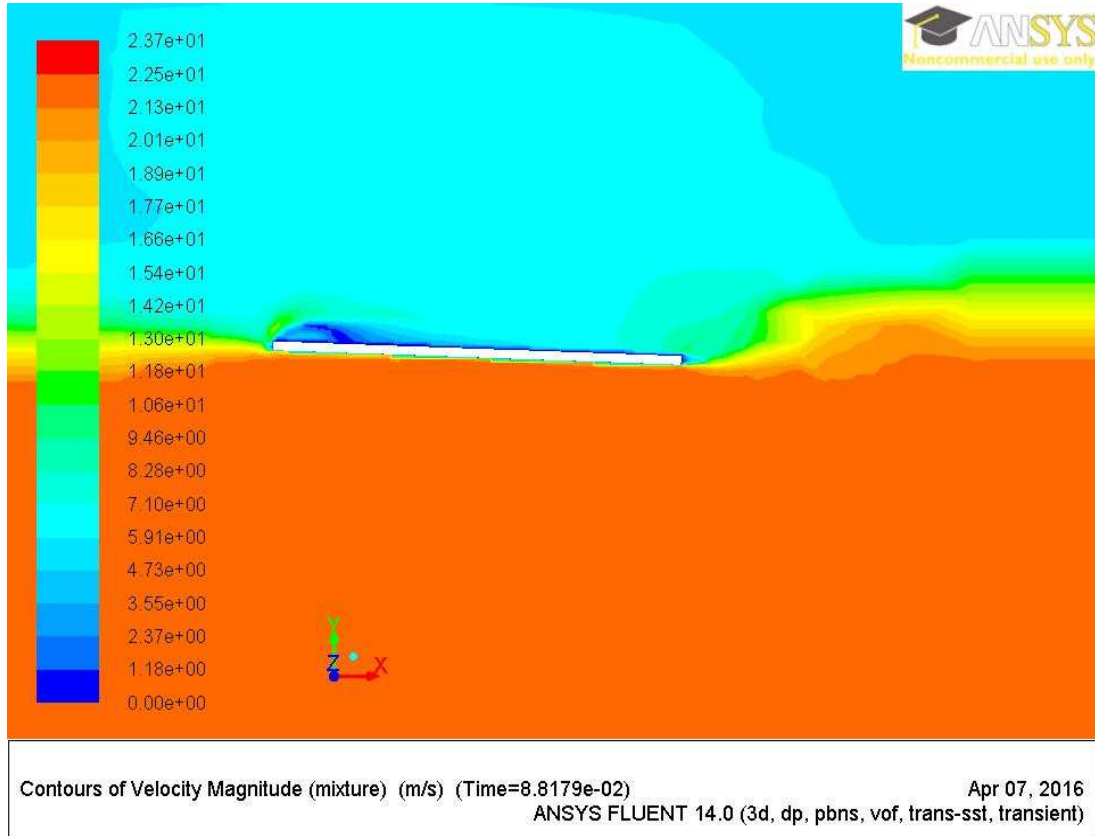


Figure 5.3: Contour of velocity at $t=0.088s$, $C_v=12.5$, $l_m/b=1.5$

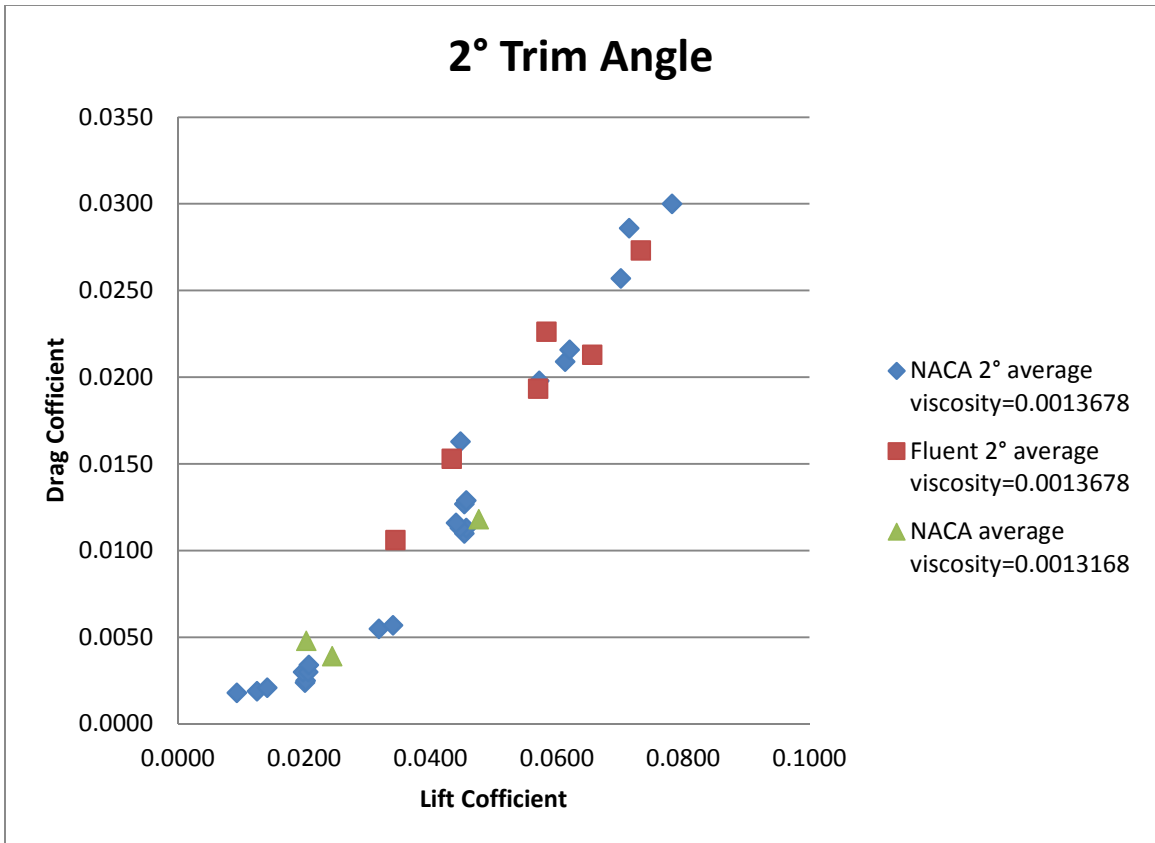


Figure 5.4: Drag vs Lift for the plate with 2° Trim Angle. Comparison of NACA and Fluent data.

Number	τ	l _m /b	C _v	2°CD _L	2°CD _b
1	2	1.5	12.5	0.0344	0.0106
2	2	3	12.5	0.0434	0.0153
3	2	4.5	12.5	0.0570	0.0193
4	2	6	12.5	0.0584	0.0226
5	2	7.5	12.5	0.0733	0.0273
6	2	3	21.7	0.0656	0.0213

Table 5.1: 2° ANSYS simulation Result

5.2 Planing Plate with 4° Trim Angle

Five cases were simulated with 4 ° trim angle. A typical wave elevation contour is presented in Fig 5.4 which shows an iso-surface of the elevation of the water (at the volume fraction 0.5). The free surface was defined as the interface between water and air where the volume fraction γ is 0.5. A comparison between the ANSYS simulation results and NACA experimental data [3] is presented in Figure 5.6 and Table 5.2. NACA experiments were performed under two different water viscosities which are marked separately in Table 5.2. Fluent simulations were performed with the viscosity 0.0013678 kg/m·s. The experimental and computational values are closely matching.

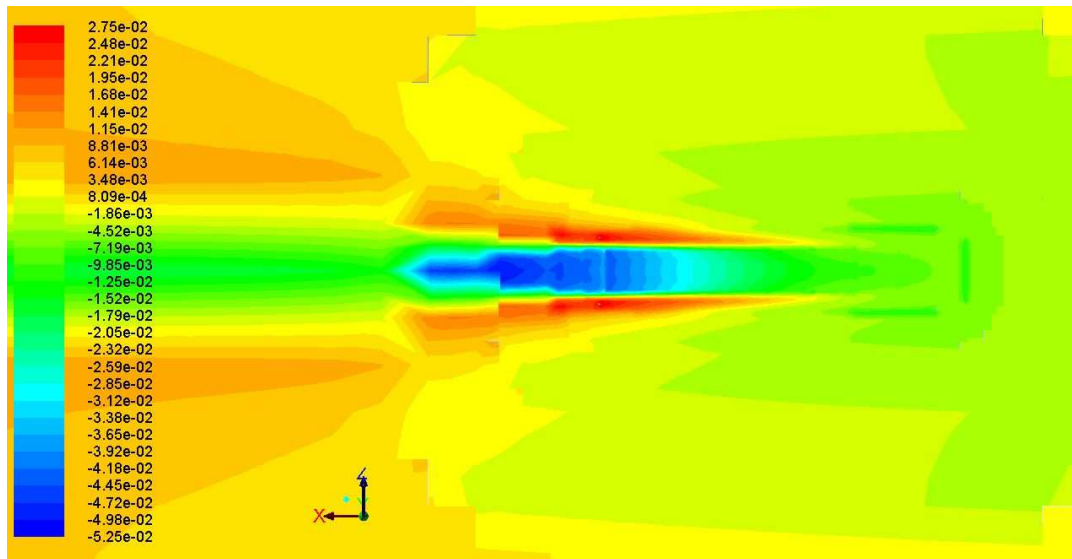


Figure 5.5: Wave Elevation Contour at $t=1.5s$, $C_v=12.5$, $l_m/b=1.5$

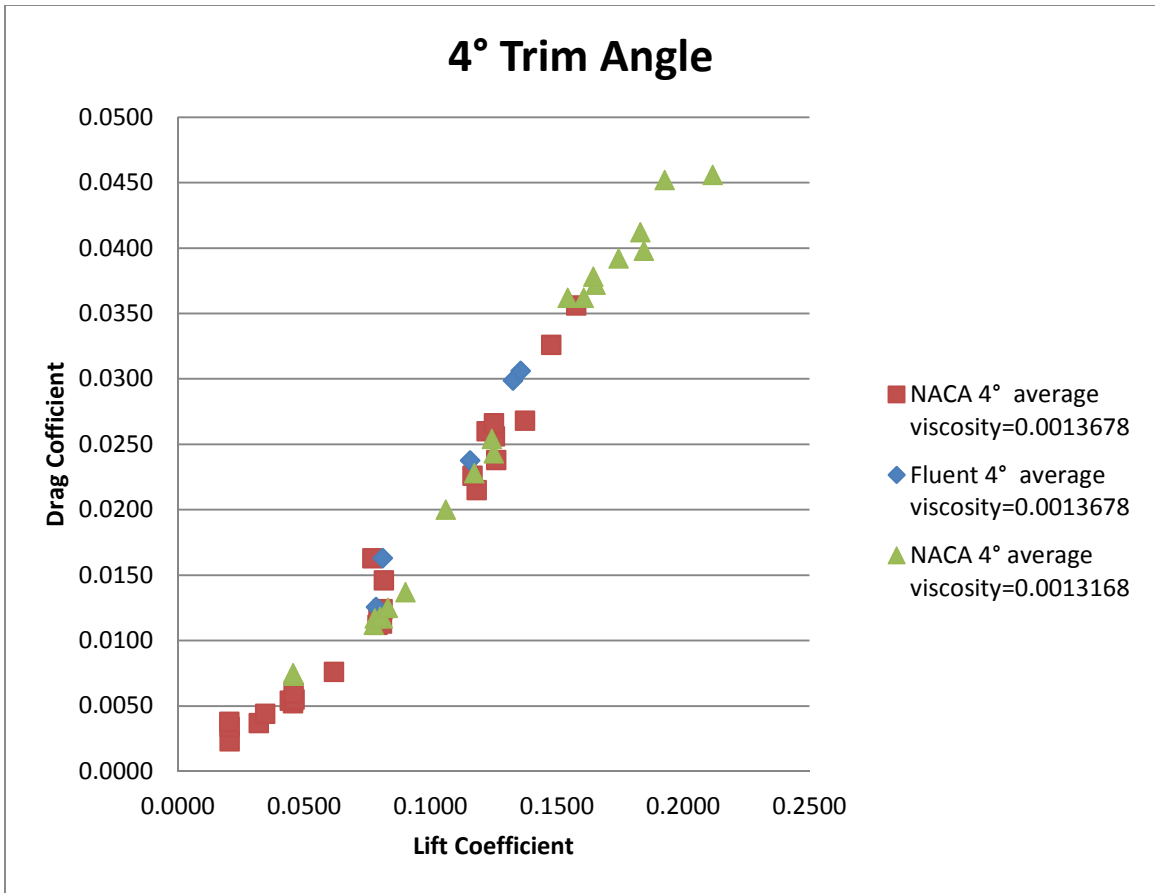


Figure 5.6: 4° Trim Angle Drag vs Lift Coefficient, comparison between NACA and Fluent.

Number	τ	lm/b	C_v	4°CD _L	4°CD _b
1	4	1.5	12.5	0.0784	0.0126
2	4	3	12.5	0.0810	0.0163
3	4	4.5	12.5	0.1156	0.0238
4	4	6	12.5	0.1325	0.0299
5	4	7.5	12.5	0.1356	0.0306

Table 5.2: 4° ANSYS simulation Result

Chapter 6

Conclusion

CFD predictions for drag and lift of a flat planing plate show good agreement with published experimental results. The study validated the use of CFD software to simulate free surface flow. However, more simulations would be suggested for the future to establish a better validation.

In this case, the NACA experiment [3] used a setup of a model and towing gear to implement the experiment, as shown in Figure 6.1. For the CFD simulation only the plate was modeled. The lift and drag from the water should thus be modeled reasonably accurately, whereas the aerodynamic forces would be expected to be less accurate. Otherwise the geometry of the planing plate, the operating conditions and the viscosity of the water were accurately modeled in the CFD simulations. The main data of interest, i.e., lift and drag, obtained from the CFD simulations matched the experimental data quite well, as shown in Figures 5.4 and 5.6.

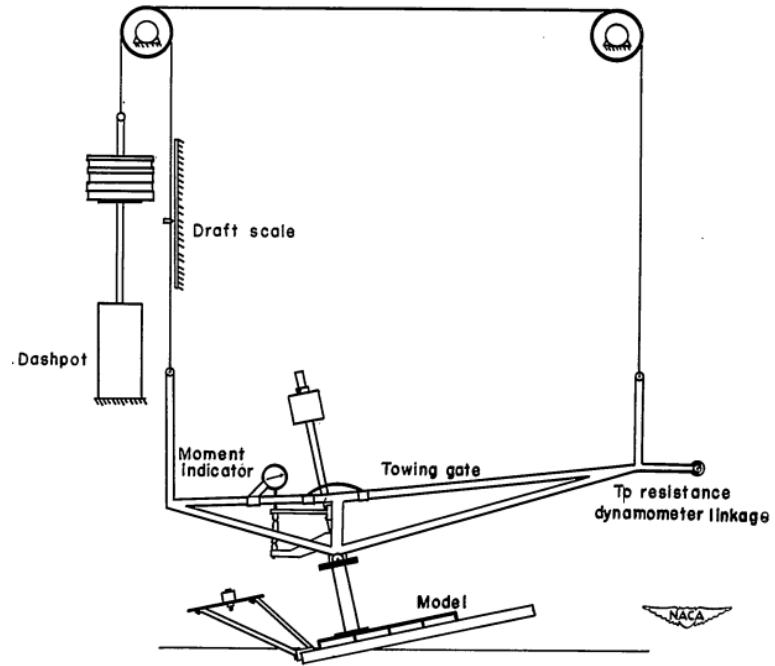


Figure 6.1: NACA Setup of model and towing gear [3]

Chapter 7

Future Work

Future work for this project would include performing more simulations under different operating conditions to see if the deviations are smaller. The mesh distribution is also a field that requires improvement. The plate in this case was set to be still which is not the real condition; rather a simulation in waves would be preferred. A dynamic mesh and control is suggested to be added in the simulation to get more practical results.

Reference

1. Truscott, Starr: The Enlarged N.A.C.A. Tank, and Some of Its Work. NACA TM 918, 1939.
2. Kapryan, Walter J., and Weinstein, Irving: The Planing Characteristics of a Surface Having a Basic Angle of Dead Rise of 20° and Horizontal Chine Flare. NACA TN 2804, 1952
3. Irving Weinstein and Walter J. Kapryan: The High-speed Planing Characteristics of A Rectangular Flat Plate Over A Wide Range of Trim and Wetted Length. NACA TN 2981, 1953
4. G.K.Batchelor. An introduction to Fluid Dynamics. Cambridge University Press. Cambridge, England. 1967
5. B.E. Launder and D.B. Spalding. Lectures in Mathematical Models of Turbulence. Academic Press, London, England, 1972.
6. Menter, F. R. Two-Equation Eddy-Viscosity Turbulence Models for Engineering Applications. The American Institute of Aeronautics and Astronautics Journal. 1994; 32(8): 1598-1605. DOI: 10.2514/3.12149.
7. White, F. M. Fluid Mechanics. 7th ed. Boston: Mc Graw-Hill; 2003.
8. Faltinsen, O. Hydrodynamics of High-Speed Marine Vehicles. New York: Cambridge University Press; 2005.
9. Wilcox, D. C. Turbulence Modeling for CFD. 3 rd ed. La Canada: DCW Industries; 2006.

10. Brizzolara, S., Serra, F. Accuracy of CFD Codes in the Prediction of Planing Surfaces Hydrodynamic Characteristics. 2nd International Conference on Marine Research and Transportation. Ischia; 2007.
11. Versteeg, H. K., Malaasekera, W. An Introduction to Computational Fluid Dynamics: The Finite Volume Method. 2nd ed. Harlow: Pearson Education Limited; 2007.
12. Larsson, L., Raven, H. C. Ship Resistance and Flow. Ed. By Paulling, J. R. Principles of Naval Architecture Series. Jersey City: Society of Naval Architects and Marine Engineers; 2010.
13. D.A. Jones and D.B. Clarke. Fluent Code Simulation of Flow around a Naval Hull: the DTMB 5415: Maritime Platforms Division Defense Science and Technology Organization; 2010.
14. Larsson, L., Stern, F., Visonneau, M. Numerical Ship Hydrodynamics An Assessment of the Gothenburg 2010 Workshop. Springer; 2013.
15. ANSYS, Inc. (2013). ANSYS FLUENT Theory Guide. Canonsburg, PA
16. ANSYS, Inc. (2013). ANSYS FLUENT User's Guide. Canonsburg, PA

Appendix A

The Mass Conservation Equation

The equation for conservation of mass, or continuity equation, can be written as follows:

$$\frac{\partial \rho}{\partial t} + \nabla \cdot (\rho \vec{v}) = S_m$$

Equation 2.1 is the general form of the mass conservation equation and is valid for both incompressible and compressible flows. The term S_m refers to the mass added to the continuous phase from the dispersed second phase (for example, due to the vaporization of liquid droplets) and any user-defined sources.

Momentum Conservation Equation

Conservation of momentum in an inertial (non-accelerating) reference frame is described by Fluid Dynamics [4].

$$\frac{\partial}{\partial t} (\rho \vec{v}) + \nabla \cdot (\rho \vec{v} \vec{v}) = -\nabla p + \nabla \cdot (\vec{\tau}) + \rho \vec{g} + \vec{F}$$

Where p is the static pressure, $\vec{\tau}$ is the stress deviation tensor (described below), and $\rho \vec{g}$ and \vec{F} are the gravitational body force and mass flux due to transportation (for example, that arise from interaction with the dispersed phase), respectively. \vec{F} also contains other model-dependent source terms such as user-defined sources.

The stress deviator tensor $\vec{\tau}$ is given by

$$\bar{\tau} = \mu \left[(\nabla \vec{v} + \nabla \vec{v}^T) - \frac{2}{3} \nabla \cdot \vec{v} I \right]$$

Where μ is the molecular viscosity, I is the unit tensor, and the second term from the right hand side arises from the effect of volume dilation.

Turbulence Modeling

The most normal way to resolve turbulence questions is to use turbulence models in which the features of turbulent flow are not solved in time. Through conducting Reynolds decomposition, the instantaneous velocity and pressure can be decomposed as

$$U_{i(x_k,t)} = \bar{U}_{i(x_k)} + u_{i(x_k,t)}$$

$$\bar{U}_{i(x_k)} = \lim_{T \rightarrow \infty} \frac{1}{T} \int_0^T U_{i(x_k,t)} dt$$

$$P = \bar{P} + p$$

Where \bar{U}_i and \bar{P} are the time averaged quantities while u_i and p are the fluctuating components of the velocities and the pressure. By inserting the Reynolds decomposition into the N-S equations, the Reynolds averaged N-S (RANS) equations are obtained as follows:

$$\frac{\partial \bar{U}_i}{\partial x_i} = 0$$

$$\bar{U}_j \frac{\partial \bar{U}_i}{\partial x_j} = -\frac{1}{\rho} \frac{\partial \bar{P}}{\partial x_i} + \nu \frac{\partial^2 \bar{U}_i}{\partial x_j \partial x_j} - \frac{\partial \overline{u_i u_j}}{\partial x_j} + g_i$$

The RANS transform equations are similar to N-S equations except for the additional term including $\overline{u_i u_j}$, referred to as the Reynolds stress tensor. If the Reynolds stress

term is modelled, the RANS equations describe the time averaged flow quantities which requires substantially less computational resources than doing DNS scenario.

A common approach for modelling the Reynolds stress tensor of the RANS equations is to use the Boussinesq approximation. In this assumption, the Reynolds stress deviator tensor is modelled as a diffusion term by introducing a turbulent viscosity, ν_t , according to:

$$-u_i u_j = \nu_t \left(\frac{\partial \bar{U}_i}{\partial x_j} + \frac{\partial \bar{U}_j}{\partial x_i} \right) - \frac{2}{3} k \delta_{ij}$$

In this equation, δ_{ij} is the Kronecker delta which assumes a value of 1 if $i=j$ and 0 otherwise, and k is the turbulent kinetic energy defined as:

$$k = \frac{1}{2} \overline{u_i u_i}$$

By using a model to describe how the turbulent viscosity depends on the flow, the RANS equations can be solved. The two-equation turbulence models, such as the k - ϵ model and the k - ω model, use two additional transport equations to describe the turbulent viscosity. They are referred to as complete models since they allow the turbulent velocity and length scales to be described independently [15].

The Standard k - ϵ Model

The standard model in ANSYS FLUENT falls within this class of models and has become the workhorse of practical engineering flow calculations in the time since it was

proposed by Launder and Spalding.[5] The standard k-ε model is a model based on model transport equations for the turbulence kinetic energy (k) and its dissipation rate (ε). The equations are as follows:

$$\frac{\partial k}{\partial t} + \frac{\partial}{\partial x_i} (k \bar{U}_i) = \frac{\partial}{\partial x_j} \left[\left(\nu + \frac{\nu_t}{\sigma_k} \right) \frac{\partial k}{\partial x_j} \right] + P_k - \varepsilon$$

$$\frac{\partial \varepsilon}{\partial t} + \frac{\partial}{\partial x_i} (\varepsilon \bar{U}_i) = \frac{\partial}{\partial x_j} \left[\left(\nu + \frac{\nu_t}{\sigma_\varepsilon} \right) \frac{\partial \varepsilon}{\partial x_j} \right] + \frac{\varepsilon}{k} (C_{\varepsilon 1} P_K - C_{\varepsilon 2} \varepsilon)$$

$$\nu_t = C_\mu \frac{k^2}{\varepsilon}$$

Where σ_k , σ_ε , $C_{\varepsilon 1}$, $C_{\varepsilon 2}$, and C_μ are model constants and P_k is the production of turbulent kinetic energy. The latter is defined as:

$$P_K = -\rho \bar{u}_i \bar{u}_j \frac{\partial \bar{U}_i}{\partial x_j}$$

and is modelled using the Boussinesq approximation.

The standard k-ε model is robust and works well in predicting free flows with small pressure gradients. It's based on the assumption that the flow is fully turbulent which means the applications are limited to high Reynolds number flows.[11] Over time, it has been proved that the standard k-ε model cannot be used to describe the wave behind moving hull in a satisfactory manner.[12]

The k- ω Model

In the k- ω model described by Wilcox [9], the transport equations for the turbulent kinetic energy and its specific dissipation, ω , are used in a similar way as for the standard k- ε model. The specific dissipation is related to the dissipation according to

$$\omega \propto \frac{\varepsilon}{k}$$

The model equations for k and ω are

$$\frac{\partial k}{\partial t} + U_i \frac{\partial k}{\partial x_i} = \frac{\partial}{\partial x_j} \left[(\nu + \sigma^* \nu_t) \frac{\partial k}{\partial x_j} \right] + \tau_{ij} \frac{\partial U_i}{\partial x_j} - \beta^* k \omega$$

$$\frac{\partial \omega}{\partial t} + U_i \frac{\partial \omega}{\partial x_i} = \frac{\partial}{\partial x_j} \left[(\nu + \sigma \nu_t) \frac{\partial \omega}{\partial x_j} \right] + \alpha \frac{\omega}{k} \tau_{ij} \frac{\partial U_i}{\partial x_j} - \beta \omega^2$$

$$\nu_t = \frac{k}{\omega}$$

Where β , β^* , σ_k^ω , σ_ω , $C_{\omega 1}$ and $C_{\omega 2}$ are model constants.

The k- ω model has the advantage that it is also valid close to walls and in regions of low turbulence which means that the transport equations can be used in the whole flow domain. A disadvantage of the k- ω model is that the results are easily affected by the choice of boundary conditions and initial states.

The SST k- ω Model

Menter [6] developed the shear stress transport (SST) model by combining the advantages of the k- ϵ and the k- ω models through the use of blending functions. In this hybrid model, the k- ω model is used along the boundary layer while the k- ϵ model, formulated on k- ω form, is used in the open channel free flow.

The SST k- ω model has performed well in many types of complex flows, such as flows with adverse pressure gradients and separating flows, where the k- ϵ or the k- ω models have given results that differ significantly from experimental data. It has been recognized for its good overall performance and it is the most commonly used turbulence model for simulations of hydrodynamics.

Boundary Layers

To characterize the flow near a wall, a dimensionless wall distance is introduced:

$$y^+ = \frac{u_* y}{\nu}$$

Where y is the distance to the wall and u_* is a friction velocity. The friction velocity is defined as

$$u_* = \sqrt{\frac{\tau_\omega}{\rho}}$$

Where τ_ω is the wall shear stress, C_f is skin friction coefficient [8].

$$\tau_{\omega} = \rho \nu \left. \frac{\partial U}{\partial y} \right|_{y=0} = C_f \cdot \frac{1}{2} \rho U_{freestream}^2$$

$$C_f = [2 \lg(Re) - 0.65]^{-2.3} \quad \text{for } Re < 10^9$$

In the boundary layer, the gradients of the flow variables in the all-normal direction are generally very large in comparison to those of the free flow. This implies that a high spatial resolution is required by the solution method in order to capture the effects near the wall. A common alternative method used to circumvent the requirement of a high spatial resolution is to use wall functions, which are empirical models used to estimate the flow variables near walls. Wall functions can also be applied when the turbulence model used in a simulation is not valid close to the wall, which for example is the case for the standard k- ϵ model. Although wall functions are undesired in computational hydrodynamics due to deviations for some types of flow, they often used for numerical reasons. Standard wall functions are based on the assumption that the boundary layer can be described as a flat plate boundary layer. This means that the time-averaged velocity can be expressed as a function of the dimensionless wall distance. In the viscous sub-layer, it can be shown that the velocity parallel to the wall is proportional to y^+ . In the fully developed turbulent sub-layer, the velocity follows the logarithm of y^+ . Between these sub-layers, in the buffer sub-layers, there is a transitional region from linear to logarithmic y^+ dependence. In order for a wall function to work properly, it should be used all the way to the fully turbulent layer which corresponds to a value of y^+ above 30. The all functions also estimate the turbulence quantities near the walls.

Appendix B

The Finite Volume Method

The stationary transport equation involving diffusion and convection of a general flow variable, ϕ , can be written as:

$$\rho U_i \frac{\partial \phi}{\partial x_i} = \frac{\partial}{\partial x_i} \left(\Gamma \frac{\partial \phi}{\partial x_i} \right) + S(\phi)$$

Where Γ is the diffusivity and S is a source term which may depend on ϕ . It can be demonstrated that the equation in Chapter 2 governing the transport of \bar{U}_i , k , ϵ , ω and γ are all written on this form. By using the FVM, this equation can be discretized as:

$$a_p \phi_p = \sum_{nb} a_{nb} \phi_{nb} + S_U$$

Where

$$a_p = \sum_{nb} a_{nb} - S_p$$

In these equations, where the summations run over all the nearest neighbors of each cell, ϕ_p is the value of the flow variable in the present cell and ϕ_{nb} are the values of the flow variable in the neighboring cells. S_U and S_p are the constant and flow variable depending parts of the source term, respectively. Furthermore, a_p is the discretization coefficient associated to the present cell. And a_{nb} are discretization coefficients describing the interaction with its neighboring cells. The discretization coefficients depend on the discretization schemes used to approximate the values of the flow variables on the cell boundaries, also known as cell faces. By using appropriate

discretization schemes to determine the coefficients of equation, a set of algebraic equations for the cell values is obtained.

Dimensionless Converge Criteria

The value of this residual can vary between different variables. In order to compare the residuals and determine convergence, they must be related to some parameters. This can be done by scaling them with an appropriate factor to make the residuals into dimensionless numbers. In FLUENT, the residuals are scaled by a characteristic flow rate of the variable ϕ in the domain. This yields a globally scaled residual, defined as

$$R_{\phi,S} = \frac{R_{\phi}}{\sum_{i=1}^N |a_p \phi_p|}$$

Besides examining the residuals, the mass, momentum and energy imbalance in each cell can be checked. It is also important to monitor the solution of important variables to determine if they reach a steady value.

Curriculum Vitae

Jennifer Gao

ManGao2015job@gmail.com • 484-725-5882 • 14 Duh Drive Apt 122, Bethlehem, PA 18015

Summary

- Four years' 2D and 3D model design experience of SolidWorks, AutoCAD, UG NX, CATIA, Pro E.
- Strong skills in manufacturing process, CFD, thermal analysis, FEA, ANSYS, FLUENT, MSC Nastran.
- Proficient in computer languages: Python, C, Java, MATLAB, Origin.

Education

May 2016 **Lehigh University, Bethlehem, PA**

Mechanical Engineering (MS)

Jun. 2014 **Shanghai Jiaotong University, Shanghai, China**

Mechanical Engineering (BS)

Work Experience

Energy Analyst Intern, Geatrain Engineering, Great New York City Area, NY

Jun. 2015 - Dec. 2015

- Performed measurements of the utility usage, equipment models, maintenance and etc. in client's work places through measuring instruments, and checked out the utility bills.
- Recommended annual energy savings to the manufacturing plants with ROI less than 10 such as VFD for motors of compressors and pumps, and air quality monitor and economizers for boilers.
- Our plan helps save 20% of client's utility expense, while the pay back period is less than 3 years and 90% of our clients adopted our recommendations and achieved the desired effect.

Propulsion System Design Assistant, Shanghai Waigaoqiao Shipbuilding CO., Shanghai, China

- May. 2013 - Sep. 2013
- Cooperated with 3 engineers in DNV and determined the initial equipment (including a main marine engine and types of belt drive) selections and arrangements in the main propulsion system according to the requirements of technical designs and operations (3100 Container Vessel).
 - Conducted and reported the design calculations and instructions of main marine engine, auxiliary machinery, shafting and piping system based on the DNV regulations.
 - Generated a report of economical efficiency using Six Sigma method for company documentation.

Research Experience

Resistance Simulation of high-speed boat Sponson, Lehigh University, PA

Sep. 2015 - May. 2016

- Utilized SolidWorks to design a 3D model of the boat sponson adjusting dead angle and hull curvature.
- Simulated the resistance of the sponson applying the Mutiphase (VOF) model in different Froude Number through ANSYS Fluent.
- Discovered the relationships between water resistance and varies Fn number.

Industrial Energy Saving Assessment (IAC Lehigh center) , Lehigh University, PA

Feb. 2015 - Aug. 2015

- Conducted a field investigation about industrial enterprises to obtain detailed statistics of energy utility.

- Measured and tracked the utility and facility service condition through comburimeter (to measure the combustion extent in the power engine), acoustic meter (to detect the gas leak in pipes and valves) and etc.
- Analyzed the statistics according to LEED applying IAC analyze packages.

Energy Saving Technology of Marine Diesel Engine Power System, Shanghai, China

Sep. 2013 - Jun. 2014

- Analyzed the main engine thermal efficiency through ANSYS, conceived and implemented performance tests of designed Waste Heat Recovery System (Supported by Man Diesel & Turbo Corporation).
- The improved system raised 15%~35% work efficiency under different work loads after equipped with WHRS, while the cost recovery period resulted in less than 10 years and completed a report for company documentation.

Hydrodynamic Model Experience with Raft Wave Energy Device, Norway, Europe

Jul. 2013 - Mar. 2014

- Evaluated hydrodynamic features of raft wave power generation devices operating under different sea conditions.
- Designed the 2D streamline diagram model in AutoCAD and simulated the numerical characteristics using Nastran.
- Conducted experiments in National Deep Water Lab with the model designed by our team.

Influence of Gas Turbine Blade Surface Roughness on Heat Transfer, Shanghai, China

Sep. 2013 - Oct. 2013

- Built and adapted the diameter and betweenness of roughness models which is hemispheres utilizing SolidWorks.
- Applied the Discrete Element Method to the entire blade and conducted numerical methods to simulate the heat transfer influence of different surface roughness model diameters and betweenness through ANSYS Fluent.
- Designed the blades according to the model from industrial enterprise through SolidWorks as comparison model.
- Conceived experiments through control variable method to discover the relationships between industrial model and laboratory model construction.